A Multi-objective Memetic Inverse Solver Reinforced by Local Optimization Methods[☆]

Ewa Gajda-Zagórska[a,b], Robert Schaefer[b], Maciej Smołka[b,*], David Pardo[c,d,e], Julen Álvarez-Aramberri[d]

[a] *IST Austria, Klosterneuburg, Austria*
[b] *AGH University of Science and Technology, Kraków, Poland*
[c] *Department of Applied Mathematics, Statistics, and Operational Research, University of the Basque Country (UPV/EHU), Leioa (Bizkaia), Spain*
[d] *Basque Center for Applied Mathematics (BCAM), Bilbao, Spain*
[e] *Ikerbasque (Basque Foundation for Sciences), Bilbao, Spain*

Abstract

We propose a new memetic strategy that can solve the multi-physics, complex inverse problems, formulated as the multi-objective optimization ones, in which objectives are misfits between the measured and simulated states of various governing processes. The multi-deme structure of the strategy allow for both, intensive, relatively cheap exploration with a moderate accuracy and more accurate search many regions of Pareto set in parallel. The special type of selection operator prefers the coherent alternative solutions, eliminating artifacts appearing in the particular processes. The additional accuracy increment is obtained by the parallel convex searches applied to the local scalarizations of the misfit vector. The strategy is dedicated for solving ill-conditioned problems, for which inverting the single physical pro-

[☆]The work presented in this paper has been partially supported by Polish National Science Centre grant no. DEC-2015/17/B/ST6/01867 and by the AGH grant no. 11.11.230.124; Ewa Gajda-Zagórska was funded by Polish National Science Centre grant no. DEC-2012/05/N/ST6/03433; D. Pardo and J. Álvarez-Aramberri were partially funded by the RISE Horizon 2020 European Project GEAGAM (644602), the Project of the Spanish Ministry of Economy and Competitiveness with reference MTM2013-40824-P, the BCAM Severo Ochoa accreditation of excellence SEV-2013-0323, and the Basque Government through the BERC 2014-2017 program and the Consolidated Research Group Grant IT649-13 on "Mathematical Modeling, Simulation, and Industrial Applications (M2SI)".

[*]Corresponding author

Email addresses: gajda@agh.edu.pl (Ewa Gajda-Zagórska), schaefer@agh.edu.pl (Robert Schaefer), smolka@agh.edu.pl (Maciej Smołka), dzubiaur@gmail.com (David Pardo), julen.alvarez.aramberri@gmail.com (Julen Álvarez-Aramberri)

cess can lead to the ambiguous results. The skill of the selection in artifact elimination is shown on the benchmark problem, while the whole strategy was applied for identification of oil deposits, where the misfits are related to various frequencies of the magnetic and electric waves of the magnetotelluric measurements.

Keywords: inverse problems, multi-objective optimization methods, memetic algorithms

---

1. Introduction

1.1. Motivation

Parametric inverse problems (IPs) for partial differential equations (PDEs) consist of restoring the values of PDE parameters (*inverse solutions*) from the known observation of their solution called *forward solution* over certain subdomains. IPs are fundamental in several applications, such as in oil and gas exploration, structure health monitoring, and cancer tissue diagnosis (see *e.g.* [1]).

The most popular mathematical formulation of IPs is in terms of global optimization problems (GOPs), where the decision variables belong to the admissible set of parameter functions representations, and the objective functionals to be minimized express the misfit between measured and simulated PDE forward solutions.

Solving IPs meets many obstacles caused by their ill-conditioning. If the ill-conditioning involves the lack of the global misfit convexity only, but still there exists a unique global minimizer, the misfit regularization (see *e.g.* [2]) can be the effective way to obtain its numerical solution. If the problem possesses more than one solution (*i.e.* the misfit is multimodal and has many global minimizers) and/or the misfit is insensitive with respect to several decision variables in the neighborhood of the global minimizer, the complex stochastic searches (see *e.g.* [3]) allow to overcome the above difficulties when solving them.

The misfit multimodality and insensitivity are generally caused by the lack of information about the phenomenon to be analyzed. It may result in a mathematical formulation of the problem that allows multiple solutions (see *e.g.* [4]) or the uncertain misfit representation due to the irreducible measurement errors (see *e.g.* [5, 6, 7]). The other obstacles are caused by artifacts that might be produced by deterministic and stochastic global optimization strategies (see *e.g.* [8]).

The most straightforward way to improve the IPs conditioning is by increasing the amount of information about the studied phenomenon. If the phenomenon is composed of multiple physical processes, then it is possible to consider many misfits simultaneously, each one associated with a separate physics. This approach leads to the multiobjective global optimization problem defined and discussed in Section 1.2.

The idea of solving ill conditioned IPs by finding Pareto solutions for misfits imposed by multiple physics is rarely described in the literature. The authors of [9] apply the inverse quantitative structure-property relationship for designing new chemical compounds. Optimal design of a magnetic pole is considered in [10]. In both cases, different objective functions are associated with two independent methods of solving the considered forward problem.

Some existing methods for the inversion of multi-physics measurements in the area of oil exploration are based on requesting that geometrical structures identified by single-physics measurements are correlated (see *e.g.* [11]). Other methods employ experimental laws such as Archie's and Gassman's equations to relate different physical measurements among each other (see *e.g.* [12, 13]). Unfortunately, the aforementioned experimental laws contain various parameters that need to be properly adjusted, which is not always possible.

The more common idea of applying multi-objective optimization for solving IPs leads only to improving the method utilized for minimizing single ill conditioned misfit. A two-objective parameter identification by genetic algorithms can be found in [14]. The second additional criterion penalizes the small diversity in the populations of candidate solutions. Another approach used in [15] consists in combining two objective functions with an immunological algorithm. These objectives become fitnesses of individuals and T-cells, respectively.

1.2. Inverse parametric problem associated with multiple physics

Te first approach intensively utilized in the sequel of this paper is related to the set of n physical processes $u^i(\omega) \in V^i$, $i = 1, \ldots, n$, which depend on the same, unknown parameter $\omega \in \mathcal{D}$. Typically, ω is a discrete representation of a distribution of some physical quantity (*e.g.* heat conductivity) on the dense domain of the forward problem. V^i are proper Sobolev spaces and $A^i(u^i(\omega)) = 0$ the relevant equations representing forward problems, where $A^i : V^i \longrightarrow (V^i)'$ is a family of differential operators from V^i to their conjugate spaces.

We are able to measure the state of all processes, which results in the vector d; $d^i \in \mathcal{O}^i$, where $\mathcal{O}^i$ are the sets of observations specific to each

physic. Next, we introduce the misfit functionals $f(d, u(\omega))$, such that $\mathcal{O}^i \times \mathcal{D} \ni (d^i, u^i(\omega)) \to f^i(d^i, u^i(\omega)) \in \mathbb{R}_+$. Each coordinate f^i represents the particular physics $i = 1, \ldots, n$.

The first multi-objective problem that represents the IPs associated with multiple physical processes dependent on the same parameter function consists of finding ω such that it minimizes all misfit functionals in the Pareto sense (see *e.g.* [16])

$$\min_{\omega \in \mathcal{D}} \{f(d, u(\omega)) : \ A(u(\omega)) = 0\}. \tag{1}$$

The above approach might be generalized to the case of many physical processes that depend on different parametric functions. Let us assume similarly that we have n physical processes $u^i(\omega^i) \in V^i$, $i = 1, \ldots, n$, which depend on a different, unknown parameter $\omega^i \in \mathcal{D}^i$ where $\mathcal{D}^i$ is the admissible set. Their states can be measured and their measurements can be denoted as previously by d; $d^i \in \mathcal{O}^i$. Now, we introduce the separate, metric *space of features* $\mathcal{F}$ that represents the phenomenon to be recognized, (*e.g.* oil deposit, tumor tissue) and the *operators extracting features* $C^i : \mathcal{D}^i \to \mathcal{F}$. The value $C^i(\omega^i)$ represents the information upon the phenomenon under interest obtained from the i-th physics. Their values may represent the characteristic function of the deposit region (*e.g.* the region of the oil occurrence).

In the sequel, we introduce a new *incidence criterion*

$$f^{n+1} : \mathcal{F}^n \to \mathbb{R}_+ \tag{2}$$

that penalizes the incoherency between the parameters assigned to the particular physics. In other words, the quantity $f^{n+1}(C^1(\omega^1), \ldots, C^n(\omega^n))$ takes a small value if the parameters $\omega^1, \ldots, \omega^n$ represent a "similar" phenomenon to be searched. As the misfit operators $f^i, i = 1, \ldots, n$, the incidence criterion is strongly related to the particular IPs. In the simplest case $n = 2$, we may set $f^3(C^1(\omega^1), C^2(\omega^2)) = \rho_{\mathcal{F}}(C^1(\omega^1), C^2(\omega^2))$, where $\rho_{\mathcal{F}}$ stands for the metric function in the space of features.

The generalized multi-objective problem that represents the IPs associated with many physical processes that depend on the different parametric functions is formulated in a way similar to the problem (1):

$$\begin{aligned} &\min_{\omega^1 \in \mathcal{D}^1, \ldots, \omega^n \in \mathcal{D}^n} \{f^1(d^1, u^1(\omega^1)), \ldots, f^n(d^n, u^n(\omega^n)), \\ &f^{n+1}(C^1(\omega^1), \ldots, C^n(\omega^n)) : A^i(u^i(\omega^i)) = 0, \, i = 1, \ldots, n\}. \end{aligned} \tag{3}$$

We foresee that, due to the last objective f^{n+1}, we will be able to seamlessly discriminate against those solutions obtained for the physical models that

are too distant. More specifically, an artifact appearing in the particular ω^i would be considered only if the other processes would yield enough evidence that the particular candidate solution is indeed promising. Thus, we expect tremendous reduction of generated artifacts and, in consequence, we expect severe reduction of multimodality of the problem (as many apparent extrema arise from interactions between artifacts and true extrema). Generally, we expect that solving many models jointly would yield information about inverse solutions that would be much broader and useful than that obtained if we considered each model separately. We hope that because of this additional information, the computational cost of solving (1) or (3) would not be larger (or, in fact, would even be possibly smaller than) the cost of minimizing each misfit separately.

Our proposed approach provides a rigorous mathematical framework that complements and generalizes existing methods for the joint inversion of multi-physical measurements. In particular, functions C^i defined above can be selected: (a) to impose some geometrical correlation, (b) to reproduce the behaviour of certain experimental laws, or (c) to impose any other interrelationship of interest between different physical phenomena.

The generalized IP formulation (3) might be considered for solving oil deposit investigations on the base of the common inverting electrical resistivity and sound speed using independent measurements obtained by the electromagnetic and ultrasonic antennas.

1.3. Paper outline

The approach presented in Section 1.2 was briefly introduced in [17]. The current paper extends the first computational experiments contained in [18] and published in [19].

We apply the complex, multi-deme Hierarchic Memetic Strategy (HMS) [20] well suited for solving IPs for finding Pareto compromise solutions of the problem (1) (see Section 2) for the case of twin physics ($n = 2$). In Section 2.2, the special kind of the selection operator, a particular type of rank selection (*cf.* MOGA [21]) that prefers the coherent Pareto solutions is discussed.

In the sequel of the paper we perform the benchmark analysis (see Section 3) showing the exploratory power of the proposed strategy and the effective elimination of incoherent compromise solutions.

The last part of the paper (see Section 4) contains the solution of a real-world engineering problem of inverting magnetotelluric (MT) measurements (see [22]) in order to find oil deposits located under the Earth's surface. Two misfit functions are related to distinct frequencies of the electric and

magnetic waves, for which the maximum sensitivity with respect to the impedance to be searched is expected. In this example, we hybridize for the first time HMS with a special kind of the local, convex optimization [23, 16] in order to increase the search accuracy.

2. Multi-Objective Hierarchic Memetic Search (HMS)

2.1. Hierarchic Memetic Search

This section contains a short description of HMS, concentrating on its computational aspects. For the details on the system architecture and algorithms, we refer the reader to papers [20] and [22].

As a whole, HMS can be seen as a composition of a global optimization tool and an external direct problem solver. The latter is necessary for the evaluation of the objectives, the former seeks the global minima of the objectives. Naturally, an integration tier must be provided for an appropriate encoding of problem parameters and the interpretation of the external solver output. The global optimization module implements a complex memetic search strategy combining a global search with high-level exploratory capabilities and an accurate as well as efficient gradient-based local search. The global part exploits ideas taken from the Hierarchic Genetic Search (HGS) [24]. Namely, the search performed in parallel by a collection of evolutionary populations. The populations, however, are not mutually independent. Instead, they form a tree-like hierarchy (see Figure 1) with a restricted number of levels. In the HGS case, such a structure proved to

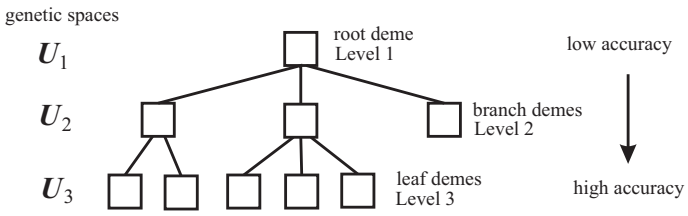

Figure 1: HMS evolutionary population tree

have considerable exploratory capabilities combined with a good search accuracy [25]. Retaining these abilities, HMS further increases the accuracy and reduces the execution time. The first goal is achieved through the application of a local optimization methods. The execution time reduction is

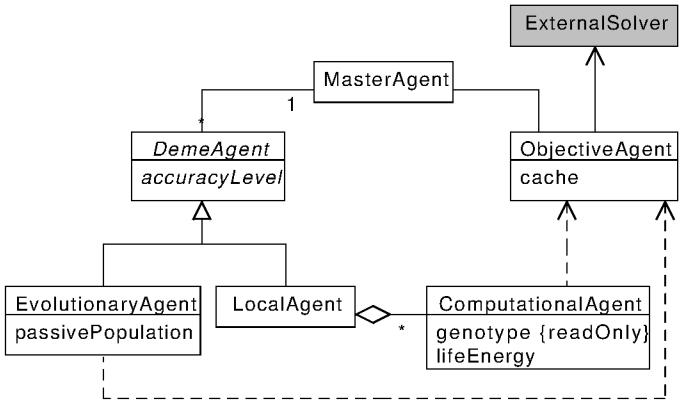

Figure 2: HMS agent types [22]

a result of a few mechanisms described in the sequel. First of all, we carefully select potential starting points for local method runs. Namely, a part of genetic individuals becomes independent agents in a multi-agent system (MAS), and the decision of performing the local search becomes their own responsibility. Evolutionary operations are appropriately adapted to such individuals (cf. [22, 26]). Moreover, the overall HMS structure is agent-based: apart from Computational Agents (CA) carrying the aforementioned 'intelligent individuals' it contains several types of managing agents (see Figure 2). This allows for a relatively easy and effective processing of the parallel evolution and synchronization of demes, and the distribution of decisions on the execution of the local method.

Master Agent (MA) is a global system manager responsible for the coordination of all demes (populations). Each running deme has its own local manager, i.e., a Deme Agent (DA). There are two types of DAs: Evolutionary Agents (EA), which are owners of simple evolutionary populations (sets of passive individuals), and Local Agents (LA), which are coordinators of active populations of CAs. Finally, Objective Agent (OA) is the objective computation coordinator. It encapsulates calls to an external solver, provides a cache for the results and can deliver a scheduler for the calls in a parallel/distributed environment.

HMS individuals of either kind located at the tree levels close to the root perform the chaotic and inaccurate search, whereas as we approach the leaves the search becomes more and more focused and the accuracy

increases (see Figure 1). The variability of the search accuracy results from the diversity of the genotype encoding precision used at different tree levels. In HMS, a real-number encoding as in [25, 27] is used (see [22]).

The variable-accuracy approach of HMS allows us to take advantage of one more solved inverse problem feature. When the dependency of the forward problem solution upon the parameters is Lipschitz-continuous and the objectives are computed by means of an adaptive Finite Element solver (*hp*-FEM) (see [28] for details), we can adapt the solver accuracy to the assumed accuracy of HMS tree demes. Each objective $f_j^i(x), i = 1, \ldots, n$ can be computed at the particular level j of the HMS tree as shown in Algorithm 1. Parameter $Ratio^i(j)$ depends on the Lipschitz constant of

Algorithm 1 Computing objective f^i using *hp*-FEM

1: solve a forward problem $A^i(u(code_j^{-1}(x))) = 0$ by *hp*-FEM for coarse and fine meshes
2: compute relative *hp*-FEM error e_{rel}
3: **while** e_{rel} is below a level-dependent $Ratio^i(j)$ **do**
4: perform one step of *hp* adaptation
5: solve $A^i(u(code_j^{-1}(x))) = 0$ by *hp*-FEM for a new fine mesh and compute a new e_{rel}
6: **end while**
7: **return** approximate objective $f_j^i(x)$ computed using the final mesh

the functional f^i, and the encoding accuracy at the j-th level of the *hp*-HMS tree. e_{rel} is a measure of the relative FEM error between subsequent steps of *hp* adaptation. Note that the aforementioned Lipschitz continuity is not obvious and it has to be proved for each particular case. For the MT problem it was proven in [22, Remark 1]. Appropriate versions for other inverse problems can be found in papers [29, 3, 30]. Furthermore, in a few important cases, we can determine the dependency between the solver accuracy and the computational cost of the forward problem solution (cf. [29, 3]), which is the main unit term of the overall HMS computational cost. Hence, by modulating the deme accuracy, we can optimize this overall cost.

2.2. Multi-objective selection and rank modification

Hierarchic Memetic Strategy for multi-objective optimization (MO-HMS) generalizes HMS by applying a multi-objective genetic algorithm in each

deme of the HMS tree (see Fig. 1). In this paper, we propose a multi-objective selection operator that builds on the Pareto-dominance ranking procedure introduced in MOGA [21] and on the rank modification idea which was originally presented in [18, 19].

In the proposed selection scheme, the rank of an individual is given as the number of solutions by which it is dominated in a particular deme. The normalized ranks are modified by applying a *rank modification* (RM) function $h_j : U_j \to \mathbb{R}_+ \cup \{0\}$. Thus, the modified fitness function $mod\_fitness_j : U_j \to \mathbb{R}_+ \cup \{0\}$ for an individual $x \in U_j$ in a particular epoch is of the form:

$$mod\_fitness_j(x) = \frac{rank(x)}{\mu_j} + h_j(x), \tag{4}$$

where $\mu_j < +\infty$ stands for the population cardinality on the j-th level of the HMS tree.

Such formulation allows for penalizing or rewarding individuals depending upon the incidence between the objectives for the solutions they represent. In this paper, we use the following two-criteria penalizing RM function:

$$h_j(x) = c \left[\frac{f_j^1(x)}{\bar{f}_j^1} - \frac{f_j^2(x)}{\bar{f}_j^2} \right]^2, \tag{5}$$

where f_j^i, $i = 1, 2$ are the objective functions induced by two physical models, $\bar{f}_j^i$, $i = 1, 2$ are the maximum observed values of objectives on the j-th level of the HMS tree, and $c \in \mathbb{R}_+$ is a constant scaling parameter.

The fitness function for incidence-based rank modification is defined as the following:

$$fitness_j(x) = \begin{cases} mod\_fitness_j(x) & \text{if} \quad 0 \leq mod\_fitness_j(x) \leq 1 \\ 1 & otherwise. \end{cases} \tag{6}$$

The main consequence of applying RM is reduction of the quantity of sprouted demes in regions with low incidence between objective functions. The number of objectives does not change, but solutions resulting from artifacts and model inaccuracies are filtered out. Therefore, better quality results can be obtained in reduced computational time. Moreover, the influence of objective incidence can be steered by parameter c in (5) or by defining a new RM function h_j.

We utilize a proportional selection, where the probability of selecting an individual is obtained from its fitness by using a validating function $g(\zeta) = 1 - \zeta$. In general, any decreasing function $g \in C([0, 1] \to [0, 1])$ can be used, depending on the desired selection pressure (see [31]).

2.3. Local search reinforcement by a gradient-based method

In paper [19] we used MO-HMS strategy exploiting only evolutionary searches. In the current paper we advance the local search abilities through the use of a gradient-based local optimization method. This is performed according to the overall HMS memetic approach, cf. [22], but we also take into account the multi-objective context. Probably the most common technique employed in solving multi-objective problems by means of local optimization methods is the objective scalarization (see, e.g., [23]). In experiments described in Section 4.2 we use the simple weighted-sum version of the technique, i.e. having selected positive numbers $w_i > 0$, we construct a new objective function

$$f = \sum_{i=1}^{n} w_i \cdot f^i. \tag{7}$$

It is well-known (cf. [23]) that the minimum of (7) is always a Pareto solution of problem (1). Moreover, if the considered problem is convex, we can obtain all Pareto solutions through the minimization of problems (7) with an appropriate variation of weights w_i (cf. [16]). Probably, it is not our case, but we do not apply any scalarization in the global search. Instead, the scalarization is used to increase the accuracy of the final solutions. Namely, we use EA-EA-LA three-level deme tree layout with Evolutionary Agents equipped with the selection operator described in Section 2.2 on the root and intermediate levels of the tree. On the other hand, on the leaf level we run active Computational Agent populations managed by Local Agents. Each of those populations receives its own separate set of weights: the same for all individuals. The problem of weight selection has been thoroughly studied (cf. [23] and the references therein). A common approach is to select something similar to

$$w_i = \frac{1}{\hat{f}^i},$$

where $\hat{f}^i$ is a quantity related to objective f^i. It can be, e.g., either a lower bound (cf. [32]) or an upper bound (cf. [33]). Of course, in general, the determination of the bounds of the objectives is highly problematic. Therefore, we rather use the objective values computed in the seed point of a particular leaf deme. This choice is justified by the fact that the leaf-level search is very focused and the probability that individuals diverge far from the initial deme center is small. Let us note that in this manner we fix a local scalarization for all the actions performed within a leaf deme: both evolutionary (hence we can use here standard HMS operators) and, more importantly, those related to the local gradient-based optimization.

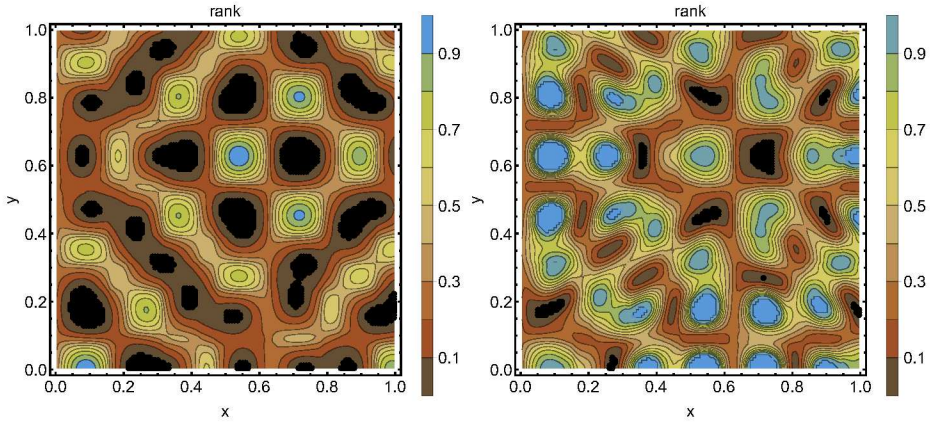

(a) (b)

Figure 3: Rank maps for MO-HMS benchmark simulations, (a) the original problem without rank modification, (b) the modified problem incorporating incidence between objectives. Ranks are calculated numerically for a mesh of sample points. Sample points with $rank < 0.02$ are denoted with black.

3. Benchmark example

Computational benchmark studies presented in this section aim at illustrating and showing the advantages of the approach presented in Section 2.2. We compare performance of MO-HMS without and with RM on a two-objective multimodal benchmark problem imitating a real-world inverse problem with objectives induced by two physics models. The goal is to find regions in which both objectives have small and similar (high incidence) values, and to filter out artifacts that appear in one objective and are not recognized in the other (lack of incidence).

3.1. Benchmark problem formulation

The problem consists of minimizing two objective functions:

$$f_1(x, y) = sin(15x)\, cos(20y) + 1, \tag{8}$$

$$f_2(x, y) = sin(20x)\, cos(15y) + 1, \tag{9}$$

where $(x, y) \in [0, 1] \times [0, 1]$. In this region, f_1 has 17 minima, from which 2 are at the boundary of the search space, and f_2 has 21 minima, from which 9 are at the boundary.

The Pareto set is not globally connected; it is composed of multiple connected parts. Figure 3a shows the shape of the Pareto landscape based

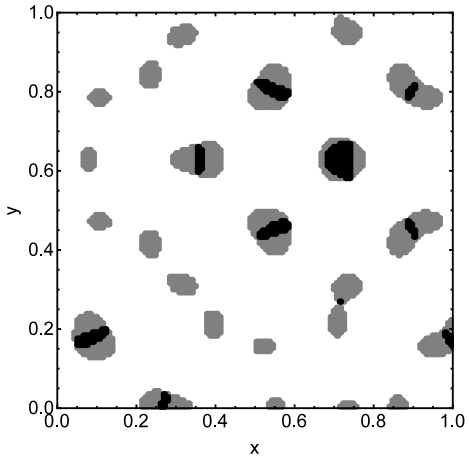

Figure 4: MO-HMS benchmark simulations. The best numerically calculated sample points for the original problem (gray dots) and for the problem incorporating incidence between objectives (black dots).

on ranks calculated numerically for a mesh of $2^l \times 2^l$ sample points with $l = 8$. Figure 3b shows ranks after incorporating incidence between objectives for the same mesh of sample points. In both figures, the neighbourhoods of the Pareto set are denoted with the black color. A comparison of these sets is presented in Figure 4. The number of connected components of the Pareto set is about 30 in the original problem and 11 in the problem incorporating incidence. There are 6 minima with very good incidence (in nearly the same place for both objective functions), from which 1 is close to the boundary, and there are additional 5 minima with good incidence (with overlapping basins of attraction, but slightly shifted optimal points).

3.2. Noise

In the considered real-world inverse problem (see Section 4), the accuracy of the forward problem *hp*-FEM solver depends on the level of the HMS tree – it is the lowest in the root and the highest in leaves. In benchmark studies, we include noise to simulate the error of the forward problem solver. Such noise is obtained by generating normally distributed random numbers based on Box-Muller transform, $Z = var\ \sqrt{-2\,ln\,U_1}\,cos(2\pi U_2)$ where $mean = 0$, variance $var = 0.2$, and U_1 and U_2 are independent random variables [34]. Thus, final calculated fitnesses $\bar{f}_i$ for $i = 1, 2$ are $\bar{f}_i(x, y) = |f_i(x, y) + \alpha\, Z_i|$, where Z_i are independent random variables with standard normal distribution generated as above, and α is a scaling parameter. The parameter α

Table 1: Parameters of MO-HMS benchmark simulations.

	Level 1	Level 2	Level 3
Population size	50	10	5
Scaling coefficients η_j	4096	128.0	1.0
Crossing rate	0.5	0.5	0.5
Mutation rate	0.1	0.02	0.004
Mutation standard deviation	0.2	0.05	0.01
Sprout distance	0.1	0.05	
Sprout standard deviation	0.05	0.005	
Sprout maximum rank	0.08	0.1	
Noise parameter α	0.5	0.2	0.0

changes depending on the level in the HMS tree: it is equal to 0.5 for the root (the biggest noise reflecting the lowest accuracy and the highest error in *hp*-FEM), 0.2 for the branches, and 0 for the leaves (no noise).

3.3. Simulations

The problem is solved with MO-HMS with 3 levels. The stopping condition is set to 50 metaepochs. Parameters of the simulations are summarized in Table 1. The sprout maximum rank parameter is a threshold preventing from sprouting around individuals that are not close to the Pareto front. We show four groups of experiments: without RM, and with RM (5) for $c = 1$, $c = 10$, and $c = 100$ (Figure 5). For each of these cases there were 100 runs of simulations.

3.4. Discussion on benchmark results

Figure 6 presents a comparison of the number of branches an leaves created during simulation. The values for RM cases are smaller, meaning that the number of sprouted demes was significantly reduced. With $c = 1$, there were about 35% less branches and 55% less leaves, and with $c = 100$ about 65% less branches and 85% less leaves. In other words, in the computed example, RM dramatically reduces the number of created leaves. This effect has a great imact in context of real-world applications, where the most significant factor of computational complexity results from accurate computations at the leaf level.

Applying RM results in filtering out solutions with low incidence between the objectives, *i.e.*, reducing the valleys of near Pareto-optimal solutions (see

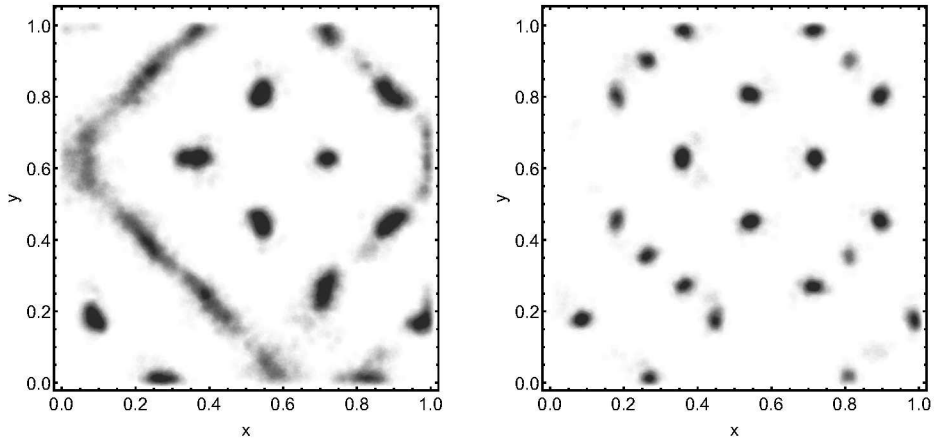

(a) No rank modification.

(b) RM with $c = 1$.

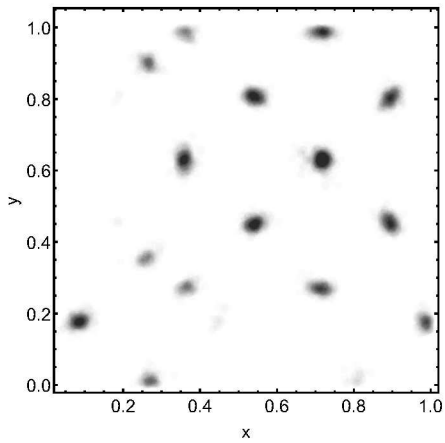

(c) RM with $c = 10$.

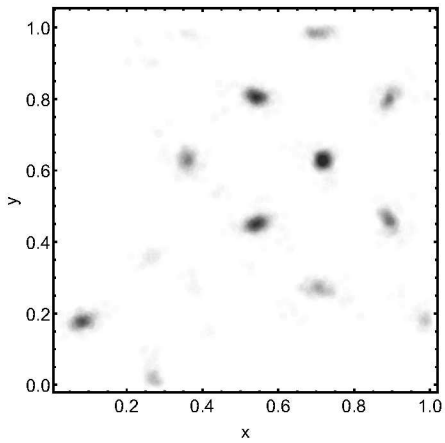

(d) RM with $c = 100$.

Figure 5: MO-HMS simulation results for four test cases. Dark colour denotes regions with high density of leaf individuals.

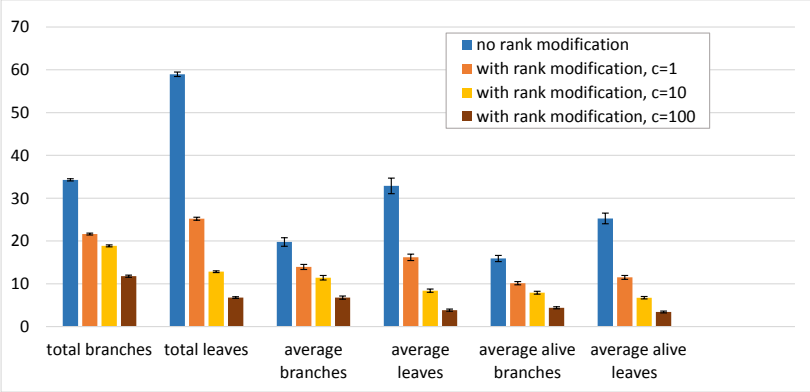

Figure 6: Average numbers of branches and leaves for 100 runs of MO-HMS benchmark simulations.

e.g. $\{0.4, 1.0\}$ to $\{0.0, 0.6\}$ and $\{0.6, 0.0\}$ in Figure 5a) to several regions (see Figure 5b), or even removing them completely for large c (cf. Figure 5d). The only regions with high density of individuals in Figure 5d are the ones representing actual solutions to the problem (cf. Figures 3b and 4).

4. Twin Objective Magnetotelluric Data Inversion

In this section we present an application of methods described in Section 2 in the solution of a real-world engineering problem of the inversion of magnetotelluric measurements. Note that here we use both the multi-objective selection operator defined in Section 2.2 and the local objective scalarization from Section 2.3.

4.1. Magnetotelluric inverse problem

The MT method is employed to recover the resistivity distribution of the Earth's subsurface, and hence, to provide an *image* of it. The theoretical foundations were established by Tikhonov [35] and Cagniard [36] in the 50's, and has been used in earthquake precursor prediction research [37, 38], groundwater monitoring [39] or CO_2 geological storage [40] among other applications.

Its main difference with other geophysical measurement acquisition methods comes from employing a natural source generated at the ionosphere [41]. This particular source produces an electromagnetic field that penetrates into the subsurface a distance that depends on its frequency and the resistivity distribution of the formation. Different antennas or receivers are located on the Earth's surface or on the oceans' bed, covering a vast area of study. The method works in a frequency range of 10^{-5}–10^{3} Hz, which allows to study depths from few meters to hundreds of kilometers with different resolutions (see *e.g.* [42]). It is easier and cheaper to record MT data than other more invasive measurements such as those obtained from marine controlled source electromagnetic or borehole logging.

Maxwell's equations govern the MT phenomena. In particular, when the formation and the source depend on two spatial variables (x, z), then two uncoupled modes can be derived, the so called *Transverse Electric* (TE) (or $\boldsymbol{E}$-polarization) and the *Transverse Magnetic* (TM) (or $\boldsymbol{H}$-polarization). We denote the vector electric and magnetic fields by $\boldsymbol{E} = (E_x, E_y, E_z)$ and $\boldsymbol{H} = (H_x, H_y, H_z)$, respectively. Hence, the TE mode is characterized by E_y, and the only nonzero components of the electromagnetic fields are (E_y, H_x, H_z), while the TM mode is characterized by H_y and the corresponding nonzero components are (H_y, E_x, E_z).

We focus here in the TE mode, and therefore in the scalar equation satisfied by $E_y(\rho)$, which is given by

$$-\boldsymbol{\nabla} \cdot (\mu^{-1} \boldsymbol{\nabla} E_y) - (\omega^2 \varepsilon - j\omega\rho^{-1}) E_y = -j\omega J_y^{imp}, \tag{10}$$

where μ is the magnetic permeability, ω the angular frequency, ε the electrical permittivity, and J_y^{imp} the impressed current source.

Since we deal with natural sources produced at the ionosphere, we have no control over the intensity of the source. Thus, instead of recording EM fields, it becomes natural to measure a physical quantity that is independent of the unknown intensity, for example, the impedance. For the TE mode, it is defined as $\mathcal{Z}_{TE} = \mathcal{Z}_{yz} = E_y/H_x$.

To numerically solve equation (10), we employ the self-adaptive multi-goal oriented *hp*-FEM, which have already being successfully employed to obtain accurate MT measurements [43, 44]. After numerically computing E_y, we calculate H_x from Maxwell's equations via postprocessing using the formula $H_x(\rho) = (j\omega\mu)^{-1}(\partial E_y(\rho)/\partial z)$. Hence, the impedance at each receiver $i = 1, \ldots, M$, is given by the following nonlinear functional

$$g^i(\rho) = j\omega\mu \frac{L^i(E_y(\rho))}{L^i\left(\dfrac{\partial E_y(\rho)}{\partial z}\right)}, \tag{11}$$

where $L^i(\cdot)$ is a linear and continuous functional [45, 46] associated to the i-th antenna and defined as:

$$L^i(E_y) = \frac{1}{|\Omega_{A^i}|} \int_{\Omega_{A^i}} E_y \, d\Omega. \tag{12}$$

Here, Ω_{A^i} corresponds to a small rectangular domain occupied by each antenna $i = 1, \ldots, M$.

We now define the misfit function as the Euclidean norm of the difference between the numerically computed and measured impedances at all receivers:

$$f(d, E_y(\rho)) = \frac{1}{2M} \sum_{i=1}^{M} \left| g^i(\rho) - d_i \right|^2, \tag{13}$$

where d_i is the impedance measured at the i-th antenna, $i = 1, \ldots, M$. This misfit function is associated with the particular frequency for which the simulated and measured impedances are obtained. For further details into the dependence between forward and inverse error that allows the effective application of *hp*-HMS stochastic inversion, we refer to [22].

In this work, we assume a regular domain $\Omega \in \mathbb{R}^2$ with a resistivity distribution that belongs to the set $\mathcal{D}$, the admissible set of resistivities on the modelling area. This is defined as $\mathcal{D} = \{\xi \in L^\infty(\Omega);\ \xi(x) = \sum_{i=1,\dots,K} \xi_i \chi_i(x),\ 0 < \xi_i^{min} \leq \xi_i \leq \xi_i^{max} < +\infty\}$. Here, $\{\chi_i\}_{i=1,\dots,n}$ is the indicator functions of a disjoint covering $\{\Omega_i\}_{i=1,\dots,K}$ such that $\bigcup_{i=1,\dots,K} \Omega_i = \Omega$, $\Omega_i \cap \Omega_j, i \neq j$.

The model problem for our numerical computations is represented in Figure 7. It consists of a subsurface resistivity area of 2500 km $\times$ 40 km with a 1D underlying media that incorporates a two dimensional inhomogeneity embedded in one of the layers. The computational domain Ω is then decomposed into four subdomains Ω_i, $i = 1, \dots, 4$ with constant resistivities $(\rho_1, \dots, \rho_4)$ inside each material, and we place seven receivers $i = 1, \dots, 7$.

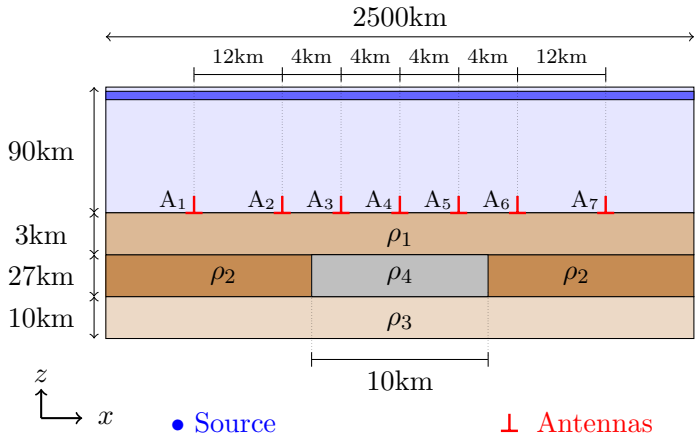

Figure 7: Geological formation and receivers location.

We employ two different frequencies, namely, $\omega_1 = 10^{-3}$ and $\omega_2 = 10^{-1.2}$ Hz. With this setting, we guarantee the best measurement conditions for both: the maximum probe sensitivity and the best penetration for a depth range 5–30 km (see [47]). Associated to the i-th frequency ($i = 1, 2$ in our case), we consider two different misfits $f^i(d^i, E_y^i(\rho))$, $i = 1, 2$ of the form of equation (13). Both misfit functions are defined over the same domain $\mathcal{D}$, and therefore, the above settings are sufficient to formulate the Pareto problem (1). This problem intends to apply MO-HMS with rank modification in order to estimate resistivities $\rho_1, \dots, \rho_4$, as described in Sections 2.1 and 2.2.

4.2. Computational results

Our quantity of interest, i.e. the impedance at the receivers, was computed by means of a goal-oriented *hp*-FEM solver (see [47] and [28] for details). In this way, we could take advantage of the ability to compute the quantity along with its first partial derivatives in a single execution. For both considered frequencies, we imposed three different solver accuracy levels: 60%, 20% and 3.5%, where the accuracy was measured as the maximal relative FEM error percentage. The reference impedance vectors d^1 and d^2 for both misfit functions were computed by solving the forward problem with the best available solver accuracy (3.2% for ω_1 and 1.2% for ω_2), assuming that the exact parameter values are $\rho_1 = 1.0$, $\rho_2 = 2.0$, $\rho_3 = 3.0$, $\rho_4 = 10.0$. As stated before, HMS had three-level deme layout with Evolutionary Agents endowed with rank-modifying MO selection at upper levels, whereas Local Agents with their active CA populations occupied the leaf level. We allowed the leaf populations to run the local optimization only once. To provide a comparison with the computations described in [19], the simulations were executed five times and the stopping conditions were set to obtain the same average number of objective calls as in the previous case. Other HMS execution parameters are summarized in Table 2.

Table 2: HMS execution parameters

	Root	Middle	Leaf
Population (initial)	20	10	5
Metaepoch length	2	2	2
Encoding scale	16384.0	128.0	1.0
Mutation rate	0.2	0.05	0.01
Crossover rate	0.5	0.5	0.5
Mutation std. dev.	3.0	0.6	0.1
Sprout std. dev.	-	1.0	0.2
Sprout min. dist.	-	1.0	0.2

As in the previous experiment, after the end of the computations, we selected the union of all obtained leaf populations, and evaluated the modified fitness (4)-(6) in this set of individuals. The comparison of stochastic solvers is not simple, because the results, especially small-budget ones, can visibly depend on the initial sampling. In Figure 8, we present the comparison of the approximate Pareto fronts obtained with (blue triangles) and without (green squares, results taken from [19]) local method executions. Both categories comprise points that had the modified fitness below 0.1. The figure

shows that HMS without local methods found one good solution and several separate solutions of slightly worse quality, while 'full' HMS (endowed with local search ability) found much more good quality solutions.

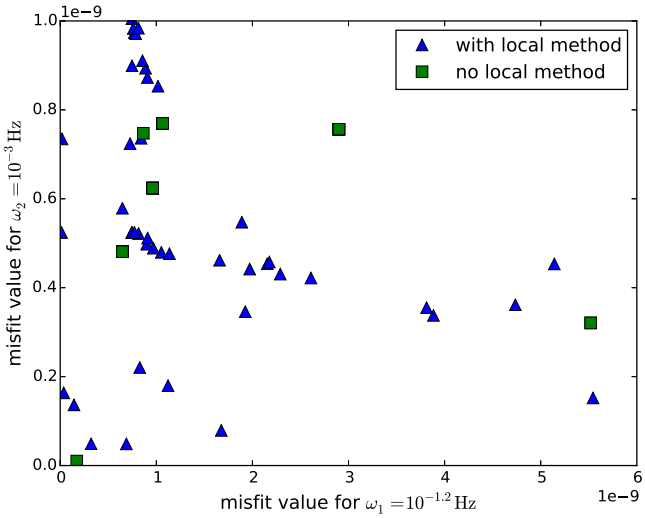

Figure 8: MT problem: Central parts of Pareto fronts (objective space)

Tables 3 and 4 show all non-dominated individuals from combined final populations for both experiments. It follows that 'full' HMS detected thrice as much best-quality solutions than any competitor in a final population.

Table 3: Non-dominated individuals (without local method)

ρ_1	ρ_2	ρ_3	ρ_4	f^1	f^2	mod. fitness
1.13084	1.89134	4.95361	3.79417	4.36966e-12	1.3282e-09	3.233923e-10
1.00934	3.35482	7.20712	5.61759	1.72058e-10	1.00846e-11	5.734588e-10

5. Conclusions

We propose a new memetic strategy for solving multi-physics, complex inverse problems formulated as multi-objective global optimization ones. The objectives are misfits between the measured and simulated states of various governing processes. The multi-deme, tree-like structure of the population allows for both, intensive and relatively cheap exploration providing

Table 4: Non-dominated individuals (with local method)

ρ_1	ρ_2	ρ_3	ρ_4	f^1	f^2	mod. fitness
1.08113	2.14728	743.6827	40424.2498	3.21456e-10	4.88782e-11	5.48761e-12
1.11638	2.26197	20.10138	1415.07494	6.88383e-10	4.87024e-11	7.94687e-12
0.98202	2.91661	0.84512	3.40328	1.43355e-10	1.36404e-10	2.92056e-10
0.974	1.33351	2925.71673	220.47357	3.68612e-11	1.63439e-10	5.00210e-10
1.00529	3.76945	25.75699	249.74075	1.42147e-11	5.24122e-10	5.35503e-9
1.385618	1.75574	1069.06592	24893.41814	8.26232e-09	1.31947e-11	1.29562e-8

moderate accuracy results and a more accurate search of some regions of Pareto set in parallel. The special type of rank selection operator prefers the coherent alternative solutions (individuals), eliminating artifacts produced by the particular processes.

The additional accuracy increment is obtained by the parallel convex searches applied to the local scalarizations of the misfit vector. The main idea of the local searches is to bound the Pareto set along the direction close to the perpendicular to the Pareto set border, so the scalarization weights are approximated locally coordinates of the normal vector. Such setting makes the local search most effective.

The strategy is dedicated for solving ill conditioned problems, for which inverting the single physical process can lead to ambiguous results.

The effect of the selection in artifact elimination is illustrated on a benchmark problem, while the whole strategy is applied for identification of oil deposits, where the misfits are related to various frequencies of the magnetic and electric waves of the magnetotelluric measurements.

The results confirm that each objective delivers partially independent information on the solutions, but the proposed rank modification delivers solutions with well balanced misfits.

Comparison of both versions of Hierarchic Memetic Search (without local methods and endowed with local search ability) shows clearly the advantage of the second one. The first strategy found one good solution and several separate solutions of slightly worse quality, while the second,'full' HMS version found three times more good quality solutions.

The computations also show that the problem is much more sensitive to shallow and vast ground layer resistivities than to deep or narrow layer ones, as physically expected.

Bibliography

[1] A. Tarantola, Inverse Problem Theory, Mathematics and its Applications, Society for Industrial and Applied Mathematics, 2005.

[2] H. Engl, M. Hanke, A. Neubauer, Regularization of Inverse Problems, Vol. 375 of Mathematics and its Applications, Springer-Verlag, Berlin Heidelberg, 1996.

[3] E. Gajda-Zagórska, R. Schaefer, M. Smołka, M. Paszyński, D. Pardo, A hybrid method for inversion of 3D DC logging measurements, Natural Computing 14 (3) (2015) 355–374. doi:10.1007/s11047-014-9440-y.

[4] E. Cabib, C. Davini, R. Chong-Quing, A problem in the optimal design of networks under transverse loading, Quarterly of Applied Mathematics 48 (2) (1990) 251–263.

[5] K. Koper, M. Wysession, D. Wiens, Multimodal function optimization with a niching genetic algorithm: A seismological example, Bulletin of the Seismological Society of America 89 (4) (1999) 978–988.

[6] V. Meruane, W. Heylen, Damage detection with parallel genetic algorithms and operational modes, Structural Health Monitoring 9 (2009) 481–496.

[7] J. M. Caicedo, G. Yun, A novel evolutionary algorithm for identifying multiple alternative solutions in model updating, Structural Health Monitoring 10 (2011) 491–501.

[8] B. Barabasz, S. Migórski, R. Schaefer, M. Paszyński, Multi-deme, twin adaptive strategy *hp*-HGS, Inverse Problems in Science and Engineering 19 (1) (2011) 3–16.

[9] N. Brown, B. McKay, J. Gasteiger, A novel workflow for the inverse QSPR problem using multiobjective optimization, Journal of Computer-Aided Molecular Design 20 (5) (2006) 333–341. doi:10.1007/s10822-006-9063-1.

[10] S. Carcangiu, P. Di Barba, A. Fanni, M. Mognaschi, A. Montisci, Comparison of multi-objective optimisation approaches for inverse magnetostatic problems, COMPEL: The International Journal for Computation and Mathematics in Electrical and Electronic Engineering 26 (2) (2007) 293–305.

[11] E. Haber, D. Oldenburg, Joint inversion: a structural approach, Inverse problems 13 (1) (1997) 63.

[12] G. Gao, A. Abubakar, T. Habashy, G. Pan, et al., Three-dimensional joint petrophysical inversion of electromagnetic and seismic data, in: 2012 SEG Annual Meeting, Society of Exploration Geophysicists, 2012.

[13] G. Pan, A. Abubakar, T. Habashy, et al., Joint inversion of borehole electromagnetic and sonic measurements, in: 2012 SEG Annual Meeting, Society of Exploration Geophysicists, 2012.

[14] M. Preuss, G. Rudolph, T. Feelly, Solving multimodal problems via multiobjective techniques with application to phase equilibrium detection, in: Proceedings of the IEEE Congress on Evolutionary Computation, 2007, CEC 2007, 2007, pp. 2703–2710.

[15] N. Chakraborti, A. Shekhar, A. Singhal, S. Chakraborty, R. Sripriya, Fluid flow in hydrocyclones optimized through multi-objective genetic algorithms, Inverse Problems in Science & Engineering 16 (8) (2008) 1023–1046.

[16] K. Miettinen, Nonlinear Multiobjective Optimization, Kluwer Academic Publishers, Boston, USA, 1999.

[17] E. Gajda-Zagórska, R. Schaefer, Multiobjective hierarchic strategy for solving inverse problems, in: IPM 2013 : proceedings of the ECCOMAS international conference on Inverse Problems in Mechanics of structures and materials, Rzeszów University of Technology Press, 2013, pp. 55–56.

[18] E. Gajda-Zagórska, Adaptive population-based algorithms for solving single- and multiobjective inverse problems, Ph.D. thesis, AGH University of Science and Technology (2015).

[19] E. Gajda-Zagórska, M. Smołka, R. Schaefer, D. Pardo, J. Álvarez-Aramberri, Multiobjective hierarchic memetic solver for inverse parametric problems, in: S. Kozieł, L. Leifsson, M. Lees, V. M. Krzizhanovskaya, J. Dongarra, P. M. A. Sloot (Eds.), International Conference on Computational Science ICCS 2015 — Computational Science at the Gates of Nature, Vol. 51 of Procedia Computer Science, Elsevier, 2015, pp. 974–983. doi:10.1016/j.procs.2015.05.239.

[20] R. Schaefer, M. Smołka, A memetic framework for solving difficult inverse problems, in: A. I. Esparcia-Alcázar, A. M. Mora (Eds.), EvoApplications 2014, Vol. 8602 of Lecture Notes in Computer Science, Springer, 2014, pp. 138–149.

[21] C. Fonseca, P. Fleming, Genetic algorithms for multiobjective optimization: Formulation, discussion and generalization, in: Proceedings of the 5th International Conference on Genetic Algorithms, Vol. 93, San Mateo, CA, USA, 1993, pp. 416–423.

[22] M. Smołka, R. Schaefer, M. Paszyński, D. Pardo, J. Álvarez-Aramberri, An agent-oriented hierarchic strategy for solving inverse problems, International Journal of Applied Mathematics and Computer Science 25 (3) (2015) 483–498. doi:10.1515/amcs-2015-0036.

[23] R. T. Marler, J. S. Arora, Function-transformation methods for multi-objective optimization, Engineering Optimization 37 (6) (2005) 551–570.

[24] R. Schaefer, J. Kołodziej, Genetic search reinforced by the population hierarchy, in: Foundations of Genetic Algorithms 7, Morgan Kaufman, 2003, pp. 383–399.

[25] B. Wierzba, A. Semczuk, J. Kołodziej, R. Schaefer, Hierarchical Genetic Strategy with real number encoding, in: Proceedings of the 6th Conference on Evolutionary Algorithms and Global Optimization, 2003, pp. 231–237.

[26] A. Byrski, R. Schaefer, M. Smołka, C. Cotta, Asymptotic guarantee of success for multi-agent memetic systems, Bulletin of the Polish Academy of Sciences: Technical Sciences 61 (1) (2013) 257–278.

[27] P. Jojczyk, R. Schaefer, Global impact balancing in the hierarchic genetic search, Computing and Informatics 28 (2) (2009) 181–193.

[28] L. Demkowicz, Computing with hp-Adaptive Finite Elements I: One and Two Dimensional Elliptic and Maxwell Problems, Applied Mathematics and Nonlinear Science, Chapman & Hall/CRC, 2006.

[29] B. Barabasz, E. Gajda-Zagórska, S. Migórski, M. Paszyński, R. Schaefer, M. Smołka, A hybrid algorithm for solving inverse problems in elasticity, International Journal of Applied Mathematics and Computer Science 24 (4) (2014) 865–886.

[30] M. Smołka, E. Gajda-Zagórska, R. Schaefer, M. Paszyński, D. Pardo, A hybrid method for inversion of 3D AC resistivity logging measurements, Applied Soft Computing 36 (2015) 442–456.

[31] E. Gajda, R. Schaefer, M. Smołka, Evolutionary multiobjective optimization algorithm as a markov system, in: R. Schaefer, C. Cotta, J. Kołodziej, G. Rudolph (Eds.), Parallel Problem Solving from Nature - PPSN XI, Vol. 6238 of Lecture Notes in Computer Science, Springer, 2010, pp. 617–626.

[32] W. Zhang, H. Yang, Efficient gradient calculation of the Pareto optimal curve in multicriteria optimization, Structural and Multidisciplinary Optimization 23 (4) (2002) 311–319.

[33] K. A. Proos, G. P. Steven, O. M. Querin, Y. M. Xie, Multicriterion evolutionary structural optimization using the weighting and the global criterion methods, AIAA Journal 39 (10) (2001) 2006–2012.

[34] G. Box, M. Muller, A note on the generation of random normal deviates, The annals of mathematical statistics 29 (2) (1958) 610–611.

[35] A. Tikhonov, On determining electrical characteristics of the deep layers of the earths crust, Soviet Mathematics — Doklady 73 (2) (1950) 295–297.

[36] L. Cagniard, Basic theory of the magneto-telluric method of geophysical prospecting, Geophysics 18 (3) (1953) 605–635.

[37] Y. Ogawa, M. Mishina, T. Goto, H. Satoh, N. Oshiman, T. Kasaya, Y. Takahashi, T. Nishitani, S. Sakanaka, M. Uyeshima, et al., Magnetotelluric imaging of fluids in intraplate earthquake zones, NE Japan back arc, Geophysical Research Letters 28 (19) (2001) 3741–3744.

[38] R. Hyndman, P. Shearer, Water in the lower continental crust: modelling magnetotelluric and seismic reflection results, Geophysical Journal International 98 (2) (1989) 343–365.

[39] P. Kantek, P. Balbi, F. Ramos, H. Fraga de Campos, Electromagnetic induction in three-dimensional structures, in: Inverse Problems in Engineering: Theory and Practice 3rd Int. Conference on Inverse Problems in Engineering, Port Ludlow, WA, USA, 1999.

[40] X. Ogaya, J. Ledo, P. Queralt, A. Marcuello, A. Quintà, First geoelectrical image of the subsurface of the Hontomín site (Spain) for CO_2 geological storage: A magnetotelluric 2D characterization, International Journal of Greenhouse Gas Control 13 (2013) 168–179.

[41] J. Weaver, Mathematical methods for geo-electromagnetic induction, Vol. 7, Research Studie, 1994.

[42] K. Vozoff, The magnetotelluric method in the exploration of sedimentary basins, Geophysics 37 (1) (1972) 98–141.

[43] J. Álvarez-Aramberri, hp-adaptive simulation and inversion of magnetotelluric measurements, Ph.D. thesis, University of Basque Country and University of Pau in MAGIQUE 3D Group (INRIA) (2015).

[44] J. Álvarez-Aramberri, D. Pardo, H. Barucq, A secondary field based *hp*-finite element method for the simulation of magnetotelluric measurements, In press in Journal of Computational Science.

[45] D. Pardo, L. Demkowicz, C. Torres-Verdín, L. Tabarovsky, A goal-oriented *hp*-adaptive finite element method with electromagnetic applications. Part I: electrostatics, International Journal for Numerical Methods in Engineering 65 (8) (2006) 1269–1309.

[46] D. Pardo, L. Demkowicz, C. Torres-Verdin, M. Paszynski, A self-adaptive goal-oriented *hp*-finite element method with electromagnetic applications. Part II: electrodynamics, Computer methods in Applied Mechanics and Engineering 196 (37) (2007) 3585–3597.

[47] J. Álvarez-Aramberri, D. Pardo, H. Barucq, Inversion of magnetotelluric measurements using multigoal oriented *hp*-adaptivity, Procedia Computer Science 18 (2013) 1564–1573.